UNIVERSIDAD REGIONAL AMAZÓNICA IKIAM

Facultad de Ciencias de la Tierra y Agua

Carrera en Geociencias

Determinación de un modelo de edad basado en el análisis de ciclicidad isotópica de ^{18}O en un núcleo de hielo del glaciar Antisana.

Jaqueline Lizeth Calero Gordon

29 de junio de 2021, ciudad de Tena, Napo, Ecuador.

CONTENIDO DEL DOCUMENTO

DERECHO DE AUTOR

Declaración de derecho de autor, autencidad y responsabilidad

Tena, 22 de febrero de 2021

Yo, Jaqueline Lizeth Calero Gordon con documento de identidad N° 1752801827, declaro que los resultados obtenidos en la investigación que presento en este documento final, previo a la obtención del título de Ingeniería en Geociencias son absolutamente inéditos, originales, auténticos y personales.

En virtud de lo cual, el contenido, criterios, opiniones, resultados, análisis, interpretaciones, conclusiones, recomendaciones y todos los demás aspectos vertidos en la presente investigación son de mi autoría y de mi absoluta responsabilidad.

Por la favorable atención a la presente, suscribo de usted,

Atentamente,

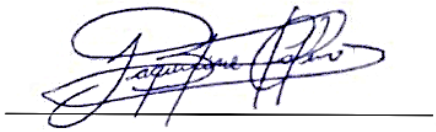

Jaqueline Lizeth Calero Gordon

CERTIFICADO DEL DIRECTOR

Certificado de dirección de trabajo de integración curricular

Certifico que el trabajo de integración curricular titulado: "**Determinación de un modelo de edad basado en el análisis de ciclicidad isotópica de ^{18}O en un núcleo de hielo del glaciar Antisana**", en la modalidad de: proyecto de investigación en formato artículo, fue realizado por: Jaqueline Lizeth Calero Gordon, bajo mi dirección.

El mismo ha sido revisado en su totalidad y analizado por la herramienta de verificación de similitud de contenido; por lo tanto, cumple con los requisitos teóricos, científicos, técnicos, metodológicos y legales establecidos por la Universidad Regional Amazónica Ikiam, para su entrega y defensa.

Tena, 17 de noviembre del 2020

Digitally signed by Bryan Valencia
Date: 2020.11.16 16:49:35 -05'00'

Bryan Guido Valencia Castillo
C.I. 6726087

Bruno Pirilo Conicelli
C.I. 1759148774

URKUND

Document Information

Analyzed document	Determination of an age model Antisana glacier Final version2.0.docx (D95908214)
Submitted	2/18/2021 3:07:00 PM
Submitted by	Bryan Valencia
Submitter email	bryan.valencia@ikiam.edu.ec
Similarity	0%
Analysis address	bryan.valencia.ikiam@analysis.urkund.com

Sources included in the report

V

AGRADECIMIENTOS

Un profundo agradecimiento a:

A PhD. Bryan Guido Valencia por haber aceptado ser mi tutor de tesis, a más de ser mi profesor es mi amigo, por su sabiduría, dedicación y paciencia ha sembrado logros en mi formación personal y académica.

A PhD. Bruno Conicelli, mi co-tutor a quien con sus enseñanzas, carácter, apoyo y confianza me asesoro hacia el mejor camino en la culminación de mi tesis.

A la Agencia Española de Cooperación Internacional para el Desarrollo (aecid) por el financiamiento de mi trabajo de titulación.

Laboratorio Nacional de Referencia del Agua (LNRA), por el almacenamiento y análisis de muestras de núcleo de hielo.

Universidad Regional Amazónica Ikiam, en especial a los docentes de la Carrera de Geociencias, quienes mediante sus enseñanzas han formado a una profesional capacitada.

Al proyecto de investigación "Estudio de la contaminación de microplásticos (Mps) en la cuenca alta del río napo: caso de estudio glaciar Antisana", la cual me apoyo en el desarrollo de mi tesis.

Al Instituto Nacional de Meteorología e Hidrológica, los/las montañistas y choferes de la Universidad, quienes estaban dispuestos en ayudar en la culminación de mi trabajo de titulación.

DEDICATORIA

A Dios por ser guía en mi camino.

A mi familia, que con su apoyo y confianza no hubiera logrado terminar mis estudios de tercer nivel.

A mis padres, Yolanda y Eduardo por ser los dos pilares fundamentales en mi vida.

A mi hermana Andrea, por ser la mayor y con el corazón tan inocente que regocijas el mío.

A mi hermano Luis, porque su carácter refleja lo contrario de su alma protectora.

A mi tía Martica Simba, que con sus alientos y actitud me dan las fuerzas necesarias para hacer lo imposible.

A mi persona, que, por mi perseverancia y forma de ser, he alcanzado muchos logros y pesar de los obstáculos y adversidades no me he rendido.

ÍNDICE GENERAL

ÍNDICE DE FIGURAS

RESUMEN

Se analizó un conjunto de datos de isótopos de oxígeno ($\delta^{18}O/ \delta^{16}O$) de un núcleo de hielo de aproximadamente 13 metros derivado del casquete glaciar sobre el volcán Antisana (0° 28'S, 78° 08'W), en Ecuador, para generar un modelo de edad basado en las fluctuaciones isotópicas. El modelo de edad inferido abarca 3,6 años, desde 1992 hasta mediados de 1995, y corresponde a 3,6 ciclos de fluctuaciones isotópicas impulsadas por el cambio estacional de las precipitaciones procedentes de la parte oriental de la región. Se realizaron transformación cuadrática (QT) y logarítmica (LT) en los datos de densidad del núcleo de hielo para remover el efecto de compresión de la nieve acumulada y corregir la señal isotópica. La transformación LT, resultó ser la más adecuada para el estudio porque redujo la gradiente natural de la densidad en función de la profundidad. Posteriormente, se evaluó al conjunto de datos isotópicos (original y ajustados) mediante funciones de autocorrelación para evidenciar ciclicidad y se validó mediante análisis wavelet. Aquí informamos de un total de 3,6 ciclos (años) que muestran que se puede derivar un modelo de edad a partir de los ciclos de isótopos de oxígeno del núcleo de hielo del Antisana. El análisis wavelet sobre los datos de LT, mostró periodicidades de 80, 40 y 20 que corresponden a ciclos de 12, 6 y 3 meses respectivamente; y confirmando que la señal periódica es constante acorde al año hidrológico. La periodicidad de 80 (un año) se repitió 3,6 veces a lo largo del conjunto de datos isotópicos. Además, la señal isotópica de LT mostró una correlación significativa con la precipitación (R^2=0.07651, p<0.001) y los datos isotópicos del núcleo de hielo del Chimborazo (R^2=0.3973, p<0.001). La metodología aplicada en este estudio demostró que se pueden derivar modelos de edad desde núcleos de hielo utilizando solamente el análisis isotópico de oxígeno en glaciares tropicales.

Palabras clave: modelo de edad, wavelet, núcleo de hielo, isotopía, ciclicidad.

X

ABSTRACT

An oxygen isotope dataset ($\delta^{18}O/\ \delta^{16}O$) from a 13-meter ice core derived from the ice cap on Antisana volcano (0° 28'S, 78° 08'W), Ecuador, was analyzed to generate an age model based on the isotopic fluctuations. The inferred age model spans 3.6 years, from 1992 to mid-1995 and corresponds to 3.6 cycles of isotopic fluctuations driven by seasonal change in precipitation from the eastern part of the region. Squaring (QT) and logarithmic (LT) transformations were performed on the ice-core density data to remove the compression effect of accumulating snow and correct the isotopic signal. The LT transformation proved to be the most suitable for the study because it reduced the natural gradient of density as a function of depth. Subsequently, the isotopic data set (original and adjusted) was evaluated by autocorrelation functions for evidence of cyclicity and validated by wavelet analysis. Here we report a total of 3.6 cycles (years) showing that an age model can be derived from the oxygen isotope cycles from the Antisana ice-core. The wavelet analysis on LT data, showed periodicities of 80, 40 and 20 corresponding to cycles of 12, 6, and 3 months respectively; and confirming that the periodic signal is constant according to the hydrological year. The periodicity of 80 (a year) was repeated 3.6 times throughout the isotopic dataset. Furthermore, the LT isotopic signal showed a significant correlation with precipitation (R^2=0.07651, p-value<0.001) and the isotopic data from the Chimborazo ice core (R^2=0.3973, p-value<0.001). The methodology applied in this study showed that age models can be derived from ice cores using only oxygen isotopic analysis in tropical glaciers.

Keywords: age model, wavelet, ice core, isotopy, cyclicity.

La revista a la cual someteré mi artículo es Journal of Glaciology

Determination of an age model based on the analysis of the isotopic ^{18}O cyclicity in an ice core of the Antisana glacier

Jaqueline L. CALERO[1]

[1]*Facultad de Ciencias de la Tierra y Agua, Universidad Regional Amazónica Ikiam, kilómetro 7, vía Muyuna, Tena, Napo, Ecuador.*

1. INTRODUCTION

Climate variability results from the interaction of the climate system components influenced by climatic factors with the potential to modulate the magnitude, intensity, of climate conditions from local to regional scales (Bradley, 1999). Generally, the study of climate variation is based on the analysis of instrumental records, satellites and climate models that provide information on rates of change and spatial-temporal evolution of climate (Basantes and others, 2016). However, there are multiple climatic processes that should be studied from paleoclimatic records in the absence of instrumental data or when the temporal scale spans beyond periods where the instrumental records are available (Bradley, 1999). Several climate studies have been developed from paleoclimatic records by analyzing their physical, chemical, or biological characteristics to reconstruct past climate and environments at different time scales, ice core records represent one of these sources of paleoclimate information that were used to infer major climatic shifts in the atmosphere, particularly those related to temperature and rainfall change (Baker and Fritz, 2015; Bradley, 1999; Sanz Rodríguez and others, 2015).

Among paleoclimatic records, ice cores are archives that record climate information in accumulating ice. The most common proxies recorded in ice cores are precipitation, air temperature, atmospheric composition, glacier retreat, evidence of volcanic eruptions, anthropogenic activity, solar activity, and source area (Bradley, 1999; Delmas, 1994; Thompson and others, 1998, 2003, 2011; Vuille and others, 2003a). The presence of anions, cations and $\delta^{18}O$ concentrations derived from ice cores, also allow the identification of droughts and rainfall events (Ginot and others, 2002; Thompson and others 1979, 1998). For this reason, ice cores are useful proxies to reconstruct palaeoenvironmental variability, especially fluctuations in rainfall (Sanz Rodríguez and others, 2015; Mosblech and others, 2012; Thompson and others, 2011; Wolff and others, 2010).

In the Neotropical Andes, precipitation seasonality, distance to water source (i.e. continentality) and convective precipitation processes over Amazon modulate the oxygen isotopic content in water vapor, this process is known as the "amount effect" (Hoffmann and others, 2003; Sturm and others, 2007; Thompson and others, 2013; Vimeux and others 2005). Additional processes influencing the isotopic composition are partial re-evaporation of water drops mixing with surrounding vapor, and adiabatic cooling favored by orographic precipitation producing a complex hydrological cycle for the tropics (Schotterer and others, 2003; Stichler and others, 2001).

On the Andes, there are studies of ice cores used for paleoclimatic reconstructions, such as Quelccaya and Huascaran in Peru, Sajama and Illinami in Bolivia, Cerro Tapado in Chile, and Chimborazo in Ecuador (e.g. Ginot and others, 2002; Henderson and others, 1999; Knüsel and others, 2003, Thompson and others, 1979, 1995, 1998). In Ecuador, the analysis from the Chimborazo record

suggested that the atmospheric conditions were governed by the Atlantic as the main sources of moisture with influence of the Pacific (Ginot and others, 2010, Vimeux and others 2009). Precipitation in Western and Eastern Ecuador depends on the moisture that is transported from Pacific Ocean and Atlantic oceans, respectively (Semiond and others, 1998). However, the moisture transported to the Eastern flank of the Andean is derived from the Atlantic Ocean, affecting differently depending on its longitudinal location and at the same influencing the accumulation of snow on Ecuadorian glaciers (Rodbell and others, 2009; Vuille and others, 2000).

Paleoclimatic studies on Ecuadorian glaciers have not yet been carried out on the same scale as in other countries such as Bolivia, Peru and Chile. Ecuadorian glaciers located on the eastern Andean flank depend on moisture derived from the Atlantic and the Amazon basin (Arnaud and others, 2001; Francou and others, 2000, 2004; Ginot and others, 2010; Basantes and others, 2016). It has been shown that moisture transport can be modulate by El Niño-Southern Oscillation (ENSO), the Intertropical Convergence Zone (ITCZ) and the South American Monsoon System (SAMS) and their interaction (Francou and others, 2004; Vuille and Werner, 2005). Inner-tropical glaciers are potential candidates in contributing to the understanding of atmospheric dynamics. In this regard, as in the case of the first palaeoclimatic studies in Huascaran, it is essential to establish an age model that determines the temporal influence of climate processes of tropical regions. The aim of this study is to determine whether the stratified ice layer in the Antisana ice cap contains a cyclic isotope signal that enables the establishment of an age model.

The Antisana volcano was selected as the object of study because this ice cap is located at low latitudes and near the Amazon basin of the equator. Moreover, suitable data such as oxygen isotopes ($\delta^{18}O/\delta^{16}O$) and density ($g \cdot cm^{-3}$) data were already available for a 13-meter ice core retrieved in 1996. The same year, the Institut de recherche pour le développement (IRD) in conjunction with the Instituto Nacional de Metereología e Hidrología (INAMHI) initiated several investigations on the Antisana Glacier 15 to understand the accumulation processes. Their efforts were centered in conducting mass balance, isotopic and ice density studies. They also concluded, based on the original data and visual observations at the time of extraction, that the record had a seasonal signature (Semiond and others, 1998). And, although they obtained ice core records, these data were not analyzed for historical interpretation.

1.1 Isotope records from tropical ice cores

According to Bradley (2015) water accumulated as snowfall is made up of oxygen and hydrogen atoms that can exist as different isotopes depending on the mass of the atomic nucleus. Atoms with equal number of protons, but different number of neutrons are isotopes of the same element. For the oxygen element, there are three stable isotopes ^{16}O, ^{17}O and ^{18}O and for the hydrogen there are two stable isotopes (^{1}H, ^{2}H). From all the possible combinations between O and H stable isotopes in a water molecule, two are the most important for climatic reconstructions $H_2{}^{16}O$ and $H_2{}^{18}O$ (Bradley, 1999). The ratio between ^{16}O and ^{18}O allows the identification of moisture source as the isotopic signature changes by fractionation processes. Therefore, the interpretation of stable isotope records in ice cores requires the identification of the source of the ^{18}O and processes affecting its variation (Yu and others, 2016).

In the Tropics, ice cores are extracted from glaciers, above the 0° isotherm, generally coinciding with the accumulation zone, where ice melting and sublimation rates are extremely low (Basantes and others, 2016; Cabrera and others, 2020) making snow accumulation continuous (Bradley, 1999) and suitable for isotopic and paleoclimatic studies (Thompson, 2000b).

At low latitudes, the relationship between the temperature signal and the $\delta^{18}O$ composition breaks down compared with areas located at high latitudes where temperatures strongly influence. Consequently, the amount of precipitation becomes the main parameter modulating the ratios between ^{16}O and ^{18}O in water vapor, a process is known as the "amount effect". In addition, along the equator, orographic configurations play an important role in the distribution and deposition of precipitation by increasing the influence of Amazonian moisture over the Andean mountains (Bradley and others, 2003; Vuille and others, 2003b).

2. STUDY AREA

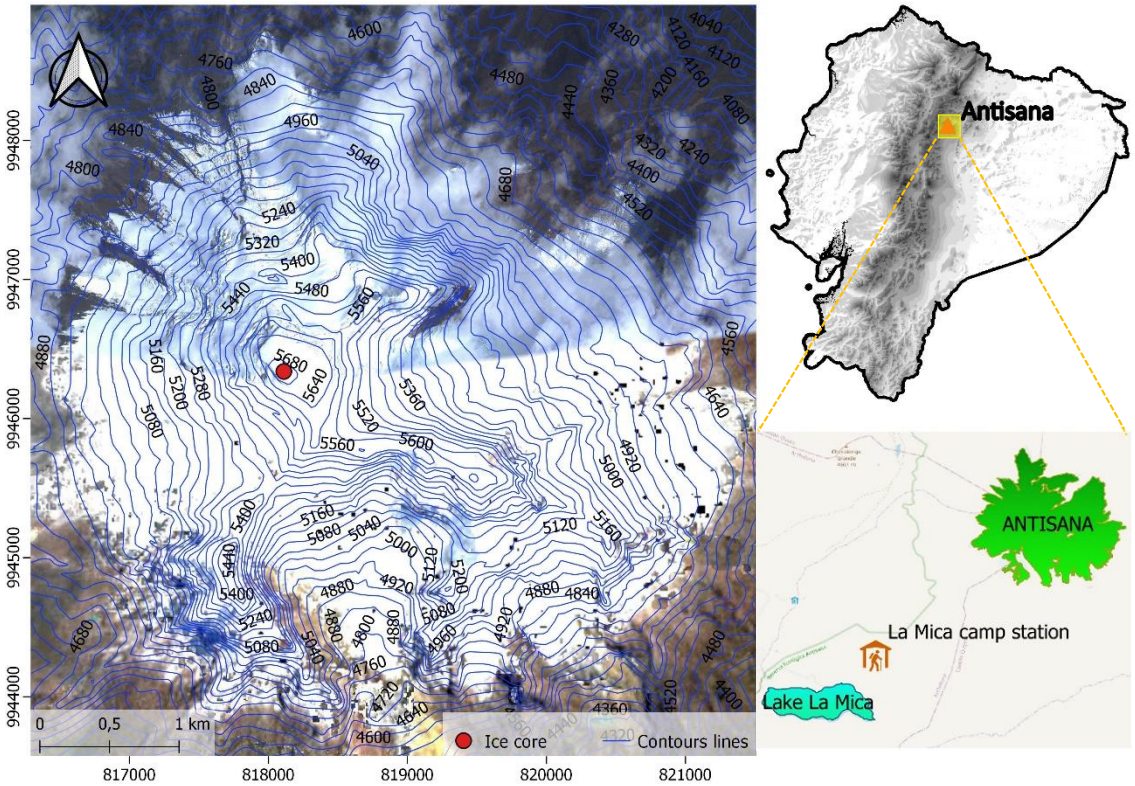

Fig. 1. Location of Antisana volcano, (left panel). Red dot, location of where the ice core was extracted, from the summit of Antisana. The blue contour lines are contour lines plotted every 40 meters and Landsat 8 is the background image source. Upper right panel shows the location of the Antisana volcano in Ecuador and lower right panel shows the location of La Mica camp station with respect to the lagoon and the ice cap (Basantes and others, 2016), where precipitation records were collected.

The ice cap (Fig. 1) lies over Antisana volcano located on the Cordillera Real of Ecuador (0° 28'S, 78° 08'W). The ice cap summit reaches 5703 m a.s.l. (Francou and others, 2000; Hall and others, 2017; Vuille and others, 2008). There is no clear precipitation seasonality in the Antisana region, due to throughout the hydrological year it presents occurrence of precipitations so there is no marked difference between dry and wet season, thus, the precipitation maximum occurs between March and May, followed by a season with less precipitation between July and October; and a second precipitation maximum in November. On the other hand, the temperature remains almost constant throughout the year at around 1˚C (Basantes and others, 2016; Favier and others, 2004; Francou and others, 2004). Since 1994, the Antisana glacier has been monitored by glaciological, meteorological and hydrological stations placed around and at different heights above the glacier (Basantes and others, 2016; Favier and others, 2004). The Antisana volcano acts as an orographic barrier blocking

atmospheric circulation and therefore precipitation mainly modulated by the Amazon basin is deposited on the ice cap, thus recording fluctuations (Garreaud and others, 2003; Thompson and others, 2000a).

3. METHODS

3.1 Data available

In February 1996, an ice core was drilled from the top of the Antisana. The work, allowed the extraction of a ~13-meter sample at the summit of the glacier that later was analyzed to estimate ice density (g·cm^{-3}) and oxygen isotope ratios of $\delta^{18}O/\ \delta^{16}O$ (Fig. 2; Semiond and others, 1998).

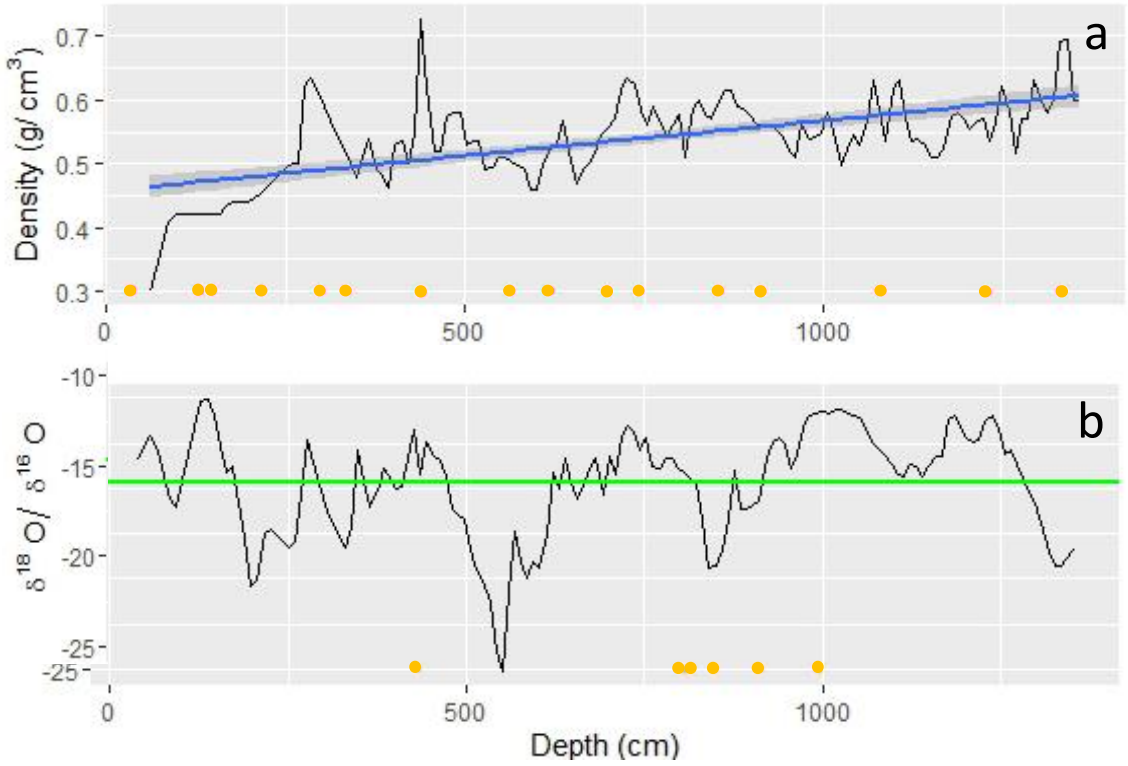

Fig. 2. Reconstruction of the density and isotopy signals recorded in the ice core. Panel (a) shows the density data in function of depth (black line) and its gradient (blue line), the deeper the depth, the higher the density, indicating the compression of the layers. Panel (b) shows the ^{18}O isotopic composition as a function of depth, the green line shows the mean of the isotope ratios (-14.72 ‰). The yellow dots in both panels depict the position of observations without data for density (points on panel a) and without isotopic data (points with on panel b).

The analysis samples taken along the core were carried out in the laboratories of the Byrd Polar Research Center of Ohio State University (USA) (Semiond and others, 1998). The density and isotopic composition were used to establish the age model.

A total of 121 samples were taken throughout the 13-meter ice core to analyze both density and isotopic composition. The first 60 and 40 cm were not considered in the density and isotopic data respectively due to gear malfunctions during the expedition. The density data presented an average of 0.54 g·cm^{-3}, with a minimum of 0.3 g·cm^{-3}, a maximum of 0.74 g·cm^{-3} and presented 16 empty observations along the core (Fig. 2a). On the other hand, the $\delta^{18}O/\ \delta^{16}O$ data showed a mean

of -14.75 ‰, a maximum of -9.52 ‰ and a minimum of -25.32 ‰ and presented 6 empty observations (Fig. 2b).

3.2 Age model design

It is known that the continuous deposition of snow on a horizontal mantle such as the summit of the Antisana volcano the force of gravity gradually deforms the underlying layers giving rise to the densification process changing its molecular structure from snow to ice, so that a density correction is necessary (Paterson, 1994). Snow compression prevented an even depth-sampling that is required to analyze the data. Therefore, transformations such as squaring (x^2; hereafter QT) and logarithm (log(x); hereafter, LT) were performed with the aim of reducing the deviation in the density gradient and thus reducing the increase in density due to the compression suffered. The transformation method for ice cores has been performed in other studies (e.g., Santibañez and others, 2018; Thorsteinsson and others, 1997). These transformations assume that snow accumulation remains constant (around 1 w.m.e.; Basantes and others, 2016) as does snow density on an annual basis. These two assumptions should still produce some distortion in the depth of the sampled data, but it should be less than the distortion produced by the compaction of the deposited ice (Herron and Langway, 1980; Nye, 1963).

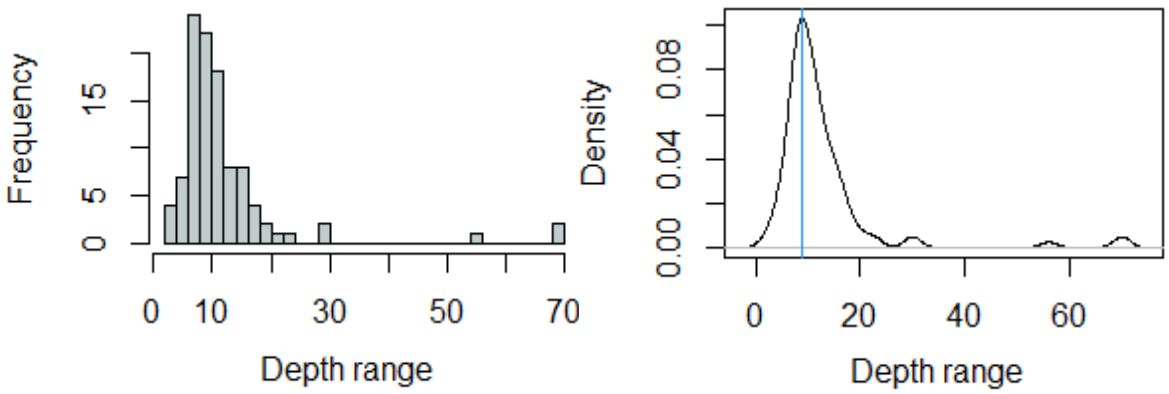

Fig. 3. Histograms and probability density functions (model) of the difference between the distance from one sampling point to the next, the most common distance was defined as the best interpolation interval. It was performed for the isotopic signal (original and adjusted).

Once the compression correction was made, the $\delta^{18}O$ isotopic data were adjusted through the transformations on density. To the 3 resulting isotopic signals, histograms and probability density functions (Fig. 3) were generated that allowed to consider the sampling points along the signals and to eliminate the influence of the absence of ice core sample data. The found value represents the most common interval (cm), which was selected as the best sampling resolution i.e., the most repeated point-to-point distance along $\delta^{18}O$ signals. Then, the depth data of the $\delta^{18}O$ signals were interpolated to the resolution found since this is a necessary requirement for performing subsequent time series analyses. Consequently, the transformed and original $\delta^{18}O$ data were analyzed through R statistical software (version 1.3.1056), autocorrelations and wavelets were applied on the transformed $\delta^{18}O$ data to learn whether the isotopic composition in the ice core was cyclic due to seasonal changes. Autocorrelations were used to measure the degree of relationship between the signal from $\delta^{18}O$ against a time-shifted copy of itself to know if the isotopic signal contained a periodic signal (Hyndman and Athanasopoulos, 2018; Kempft-Leonard, 2004). On the other hand, for wavelet analysis, the statistical package WaveletComp was used to decompose the time series within the time-frequency space based on the principles of Fourier series (Lau and Weng, 1995).

Wavelet analysis results of the comparison between the time-series signal (i.e. a signal with a constant temporal resolution) against a non-periodic wave with data centered around the mean and a finite duration that is called wavelet. This wavelet is rescaled and shifted to decompose the original signal into time and frequency components (Torrence and Compo, 1998). Wavelet analysis has been performed on sediment cores for paleoecological studies (Nascimiento and others, 2020; Moy and others, 2002); however, it has not yet been performed on ice cores.

3.3 Validation

The transformed $\delta^{18}O$ signal evidencing periodicity was correlated with precipitation data ($p/^{18}O$) recorded by German pump-pluviographs recording information from the La Mica camp station, located southwest of Antisana belonging to the Empresa Metropolitana de Agua Potable y Saneamiento de Quito (EPMAAPS) available from 1984 to 1998 and with the isotopic signal from the ice core (A-1999) drilled from Chimborazo (to 132 km SW of Antisana) with a chronology from 1987 to 1999 and from which the isotopic composition was analyzed, anions and cations (Ginot and others, 2010) in order to validate the results of the reconstruction performed on the Antisana.

4. RESULTS

4.1 Squared and logaritmic transformation

The depth of the density graph was transformed using a squaring (x^2) and natural logarithm (log(x) function; Fig. 4a and 4b) to eliminate compression in the ice core density to obtain an adjusted depth for subsequently perform autocorrelation functions and wavelet analysis. In Fig. 4a, the blue line shows the gradient at y = 7E-08x + 0.4925 with a coefficient of determination R^2 =0.296 and in Fig. 4b, it is shown at y = 0.065x + 0.1225 with a coefficient of determination R^2 = 0.518.

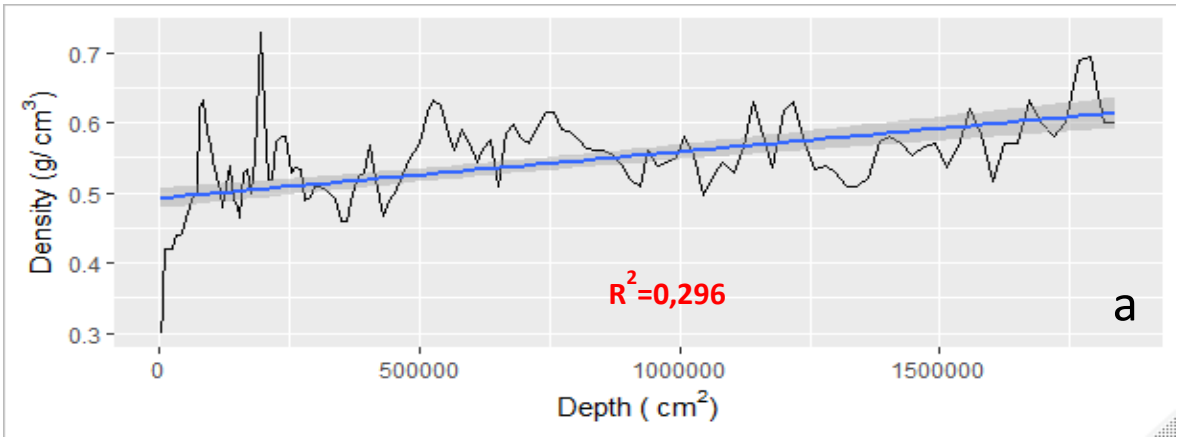

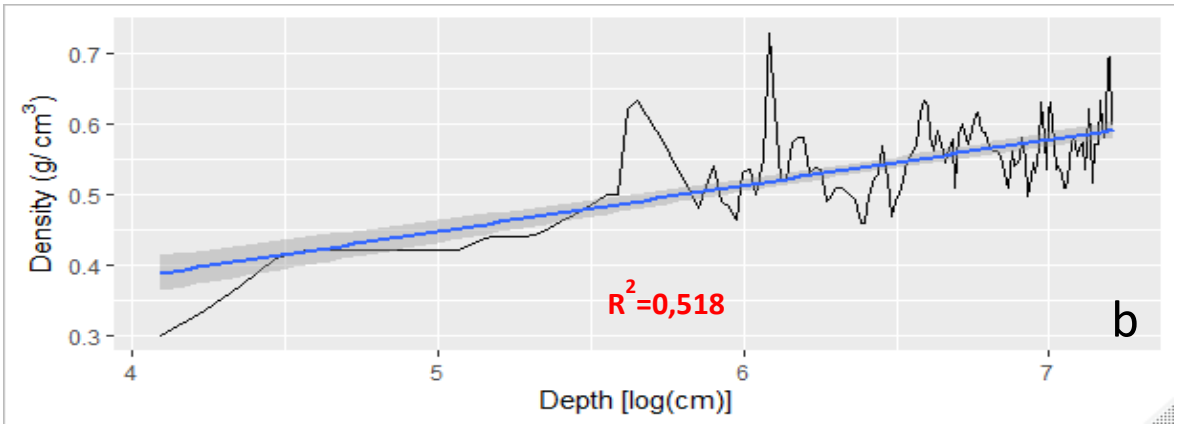

Fig. 4. Depth transformations in density data. Sampling points (depth) adjusted to the square (x^2) and the logarithm (log (x)) of the density signal drilled in 1996. Panel a shows the plot of the squared density as a function of depth (black line). Panel b shows the plot of the natural logarithm of the density as function of depth.

Thus, once the compression was adjusted for the density, the same procedure was performed for the isotope depths using the QT and LT transformations (Fig. 5a and 5b).

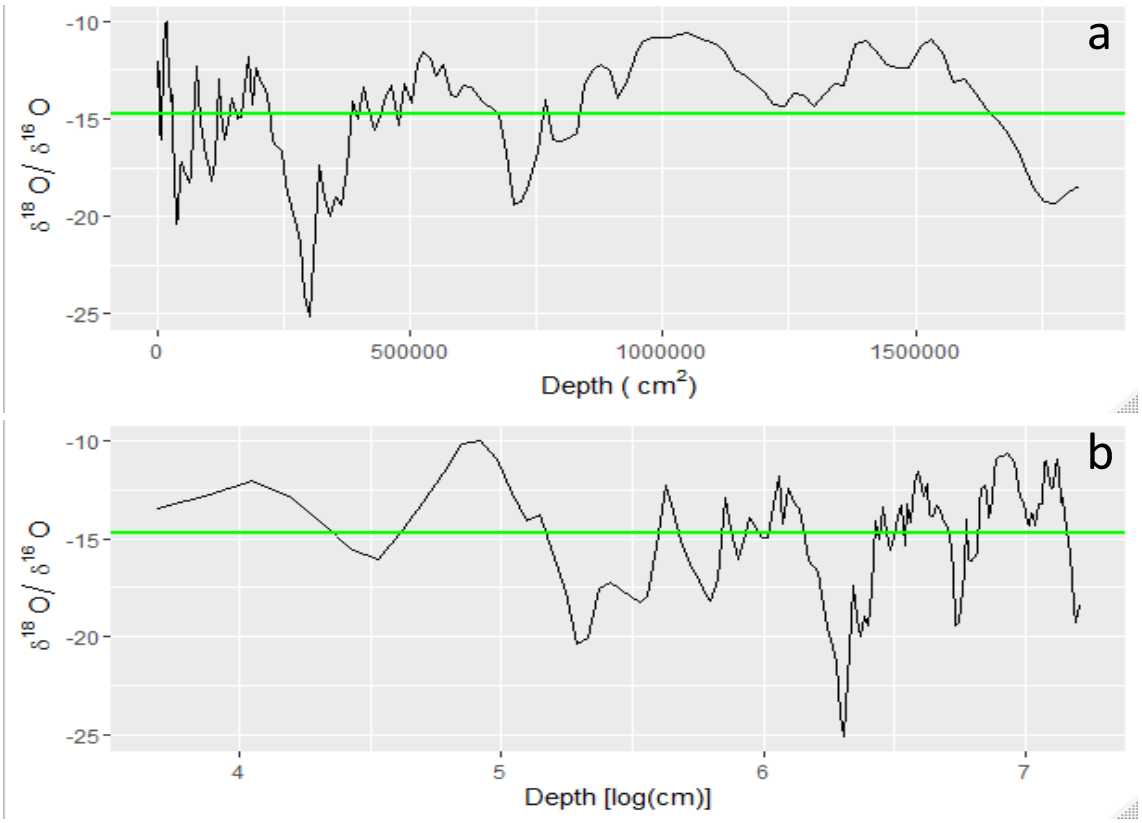

Fig. 5. Depth transformations in isotope data**.** Panel a shows the plot of the squared isotopic as a function of depth (black line). Panel b shows the plot of the natural logarithm of the isotopic as function of depth. The green line shows the average isotope record of -14.72 ‰, for both plots.

4.2 Autocorrelation functions and Wavelets analysis

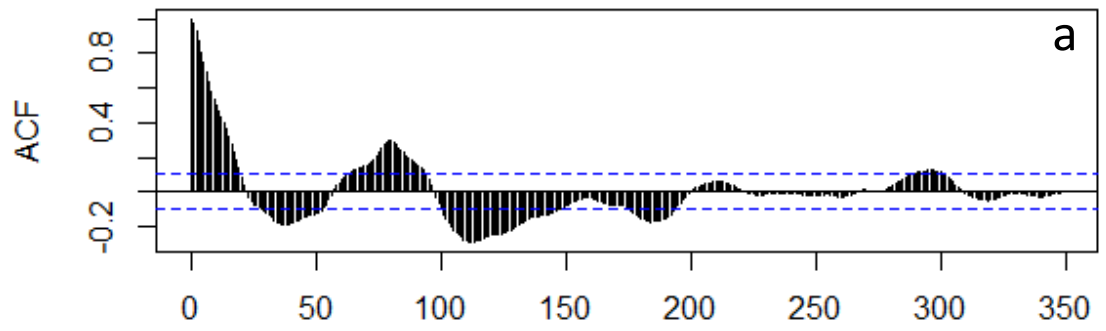

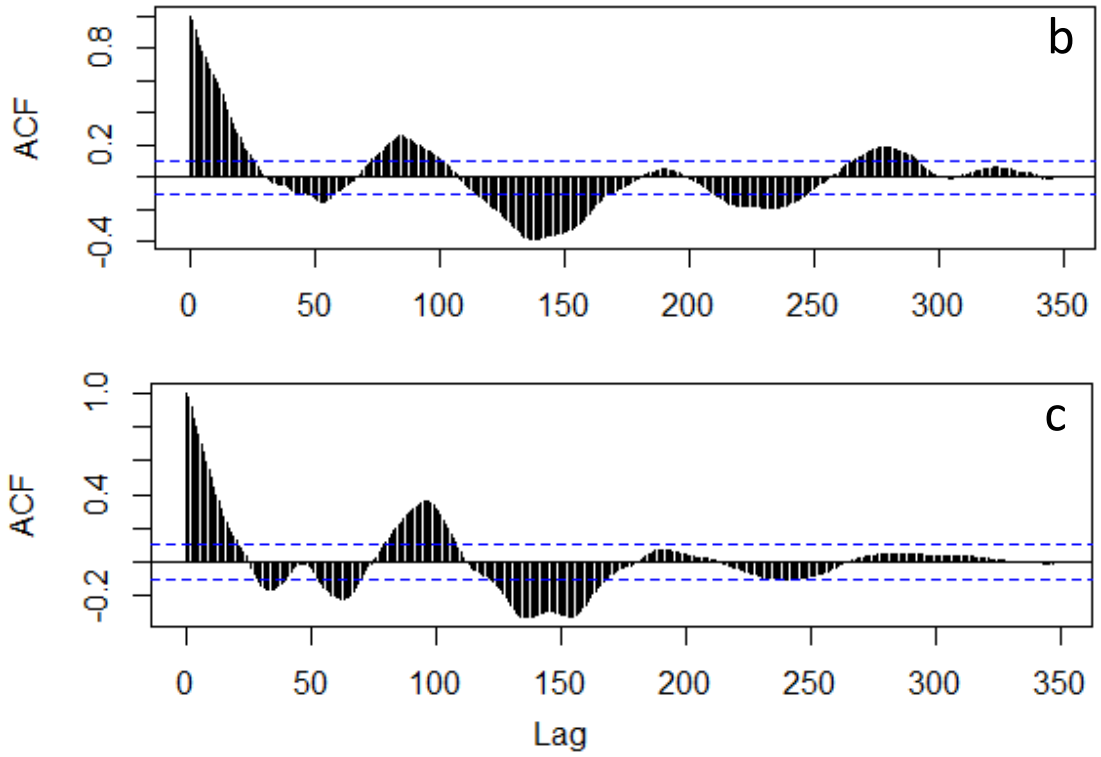

Fig. 6. Autocorrelations functions (ACF) for isotopic data. Panel a) shows the ACF for the original isotopic signal. Panel b) shows the squared transformation of the isotopic signal. Panel c) shows the logarithmic transformation of the isotopic signal. The ACF include blue dashed lines depicting the coefficients that were significant (i.e. the 95% confidence interval, CI). Values above the blue dashed line in the positive y-axis are significant, as well as values below the blue dashed line in the negative y-axis.

Autocorrelation functions rely on the correlation between a time series signal with itself (Fig. 6). A copy of the time series is displaced one step at the time (lag) starting with a lag= zero that produces an autocorrelation coefficient r_0=1, i.e. a correlation with itself without lags (Hyndman and Athanasopoulos, 2018; Kempft-Leonard, 2004). Each time series (Fig. 6a-c) contains a total of 350 observations for the original data and the transformed data (QT and LT respectively). The ACF vertical black bars represent a correlation instance between the isotope signal against itself shifted one step at the time. As additional lags are introduced in the computation, the subsequent coefficients will gradually decrease below the 95% confidence interval (CI; region between the blue dotted lines in Fig. 6). Cycles are depicted by the peak of the coefficients that extent beyond the 95% CI. Eventually, the coefficients remain below the 95% CI interval and the correlations coefficients become uninformative and non-significant (Hyndman and Athanasopoulos, 2018).

The ACF were run as a preliminary analysis, showing that the oxygen isotopic signal contained a periodic signal (Fig. 6a-c) suggesting precipitation-driven cycles could be identified. However, theses analyses are unsuitable to make proper comparisons between signals. Then, wavelet analyses were used to decompose the isotopic time series in time-frequency space (Fig. 7 a-c) and to determine if the transformed isotopic signals contained periodic cycles (Torrens and Compo, 1998). The wavelet analysis was run using the three signals (original, QT and LT). The heatmap represents the time-frequency space where the frequency of the time series is depicted on the X-axis (analogous to the time series temporal resolution) and the periodicity on the Y-axis. The limit between the white-shaded and unshaded region represents the Cone of Influence (COI). White-shaded regions cannot be used for interpretation (Cabodi and others, 2016). In the heatmap, areas surrounded by white

solid lines correspond to regions of high significance above 0.05 (red dots in the panel of average wavelet power) or 0.1 (blue dots in the panel of average wavelet power).

For the original signal, the wavelet analysis (Fig. 7a, left) showed two sets of periodicities with a power average equal to 32 and 18 (Fig. 7a, right). Similarly, the QT signal had two significant periodicities (Fig. 7b, left) with a power average of 46 and 21 (Fig. 7b, right). However, the LT signal (Fig. 7c, left), showed three significant periodicities with a power average of 80, 40 and 20 (Fig. 7c, right). The temporal consistency of the periods is depicted as a line in the panel of average wavelet power marked with blue and red dots based on its significance. The period observed at 80 had the highest average wavelet power (right panel in Fig 7c) represented by a near straight black line in the heatmap implying a constant periodicity. A black line towards higher periods in the heatmap (Fig. 7b) indicates that the periods are gaining amplitude, which is unexpected for a hydrological year. Conversely, a line towards smaller periods (Fig. 7a) indicates the periods are reducing their amplitude, which again, is unlikely for a hydrological year.

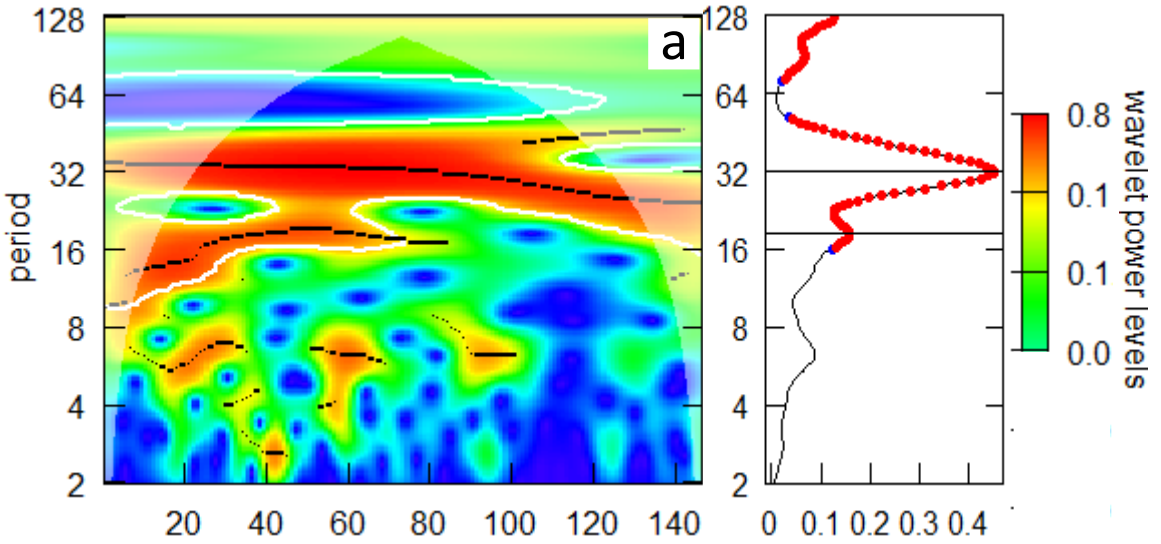

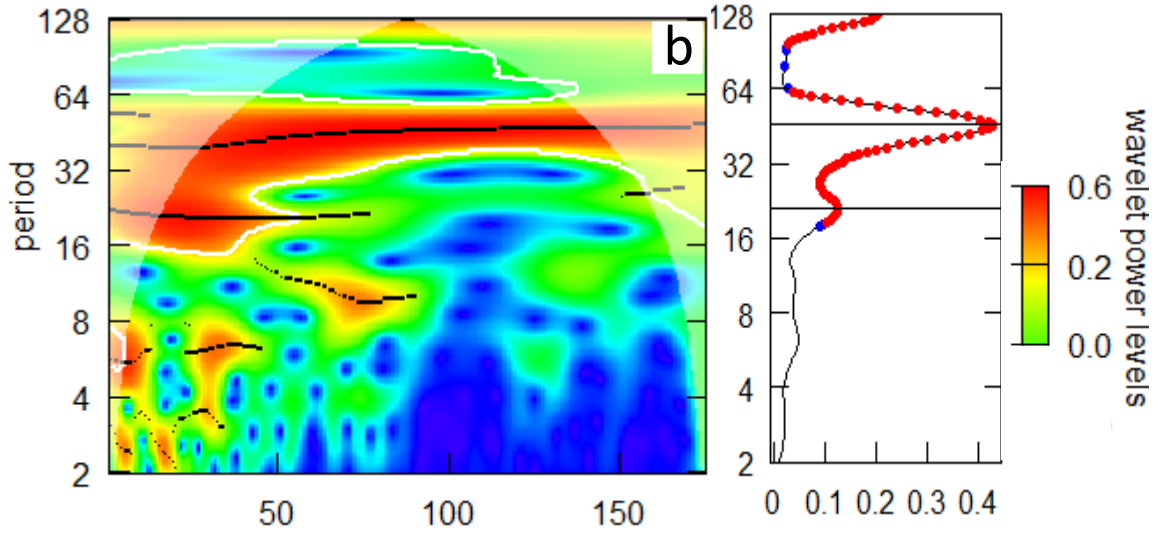

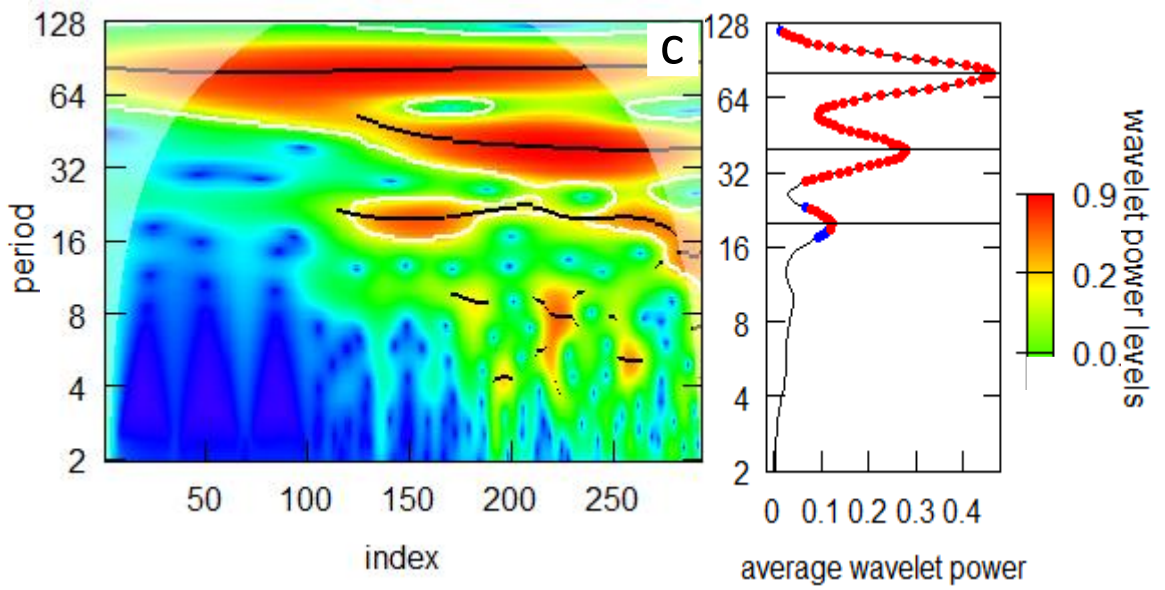

Fig. 7. Wavelet analysis of original and transformed isotopic signals. Panel a) shows the wavelet for the original isotopic signal. Panel b) shows the wavelet for the squared transformation. Panel c) shows the wavelet for the logarithmic transformation. The black lines in the heatmap represent the period highest power.

According to the wavelet analysis, the signal that best represents defined and constant periods is the logarithmically adjusted signal (LT, Fig. 7c). A reconstruction of the periodicity found in the LT wavelet is depicted as a red curve (Fig. 8) that matches the LT signal. Note that the reconstruction was significant and matches the highest average wavelet power at periodicity= 80 (red dot at the highest value of the average wavelet power in Fig. 7c).

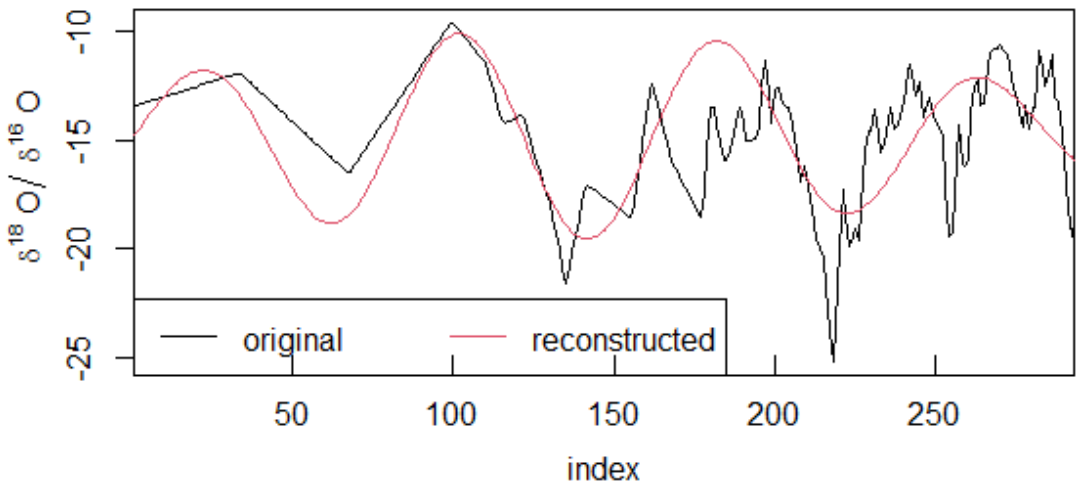

Fig. 8. Reconstructed periodicity contained in the LT signal. The x axis (index) represents the resolution of the time series. The oxygen isotope ratio is shown on the Y-axis. The red line represents the reconstructed signal (3.6 cycles) for the LT data (black line), with an average wavelet power equal to 80.

4.3 Validation of the model

Based on the ACF and wavelet analysis, it has been shown that the isotopic data of the core drilled from the Antisana glacier has periodic signal. To validate the results, the oxygen isotope signal

corresponding to the LT was correlated with precipitation recorded in a camp station located southwest from the Antisana by EPMAAPS, near Lake La Mica (Fig. 1). Monthly precipitation data were available from 1984 to September 1998. Precipitation data from 1992 to 1995 were used to correlate with the oxygen isotopic signal. The correlation between the isotopic signal and precipitation data was negative and significant (Fig. 9), r= -0.29, R^2=0.0765 and p-value<0.001, for dates 1992/01 to 1995/10.

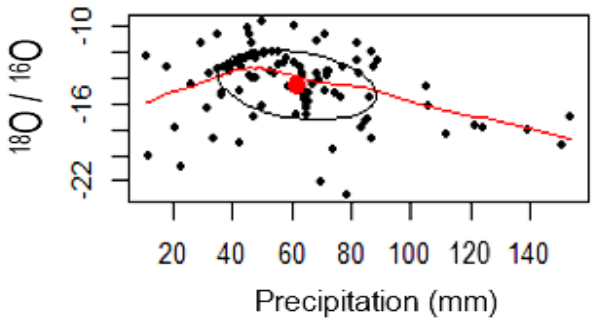

Fig. 9. Relationship between the LT signal and the monthly precipitation records extracted from the pluviograph at the La Mica camp (EPMAAPS).

The logarithmic transformed data from the Antisana was also correlated with the oxygen isotopic record from the Chimborazo glacier (Ginot and others, 2010). To perform the correlation, the Chimborazo isotopic data was sectioned and resampled to match the age range (1992-1995) and the temporal resolution (80 observations per year) of the Antisana record. The 80 observations per year represents the periodicity with highest average power found in Fig. 7c. The resample was to performed to minimize spurious correlation results. The correlation between the Antisana and Chimborazo records was positive and significant r = 0.67, R^2= 0.3973 and p-value<0.001 (Fig. 10). The reconstructed signal that corresponds to the highest significant peak in the average wavelet power was also plotted as a dotted line to show the correspondence with the Antisana and Chimborazo data (Fig. 10). The dashed black line represents the cycle contained in the Antisana isotopic data, spanning 3.6 cycles derived from wavelet analysis using the log-transformed data.

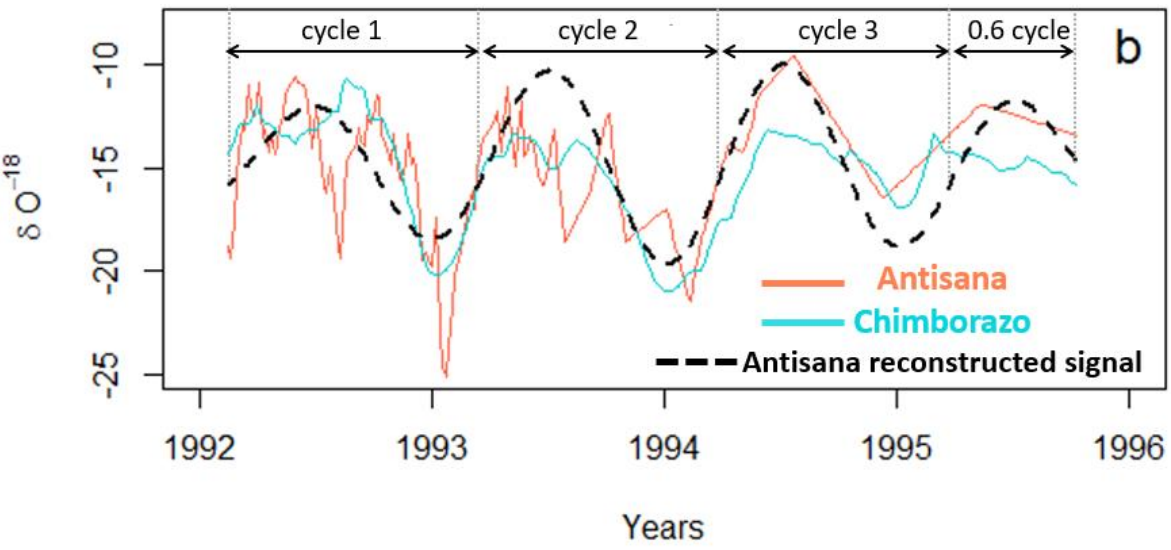

Fig. 10. Isotopic correspondence between the Antisana and Chimborazo records. Oxygen isotope data ($\delta^{18}O/\delta^{16}O$) derived from the Antisana (This study) and Chimborazo (Ginot and others, 2010) ice core records used for correlations are depicted in the diagram. The correlation between these records was significant (r= 0.67 and p-value<0.001). The reconstructed signal derived from the Antisana wavelet analysis is depicted as a

dashed black line. The span of the individual cycles was depicted with arrows. The chronology depicted on the x-axis chronology corresponds to the Chimborazo dataset that was extracted from (Ginot and others, 2010).

5. DISCUSSION

The methodology we applied was oriented to determine if periodic cycles could be identified through oxygen isotopes in an ice core extracted from the Antisana glacier to generate an age model. On annual time scales, changes in precipitation (i.e. change from dry to wet season or vice versa) are responsible for the largest isotopic fluctuation recorded in glaciers such as Antisana due to fractionation processes also known as amount effect (Baker and Fritz, 2015; Baker and others, 2009; Ginot and others, 2010; Hestenrath and others, 2004; Kellerhals and others, 2010; Mosblech and others, 2012; Schotterer and others, 2003; Stichler and other, 2001; Thompson and others, 2011, 2013; Villacís and others, 2008; Vuille and others, 2003a, 2003b). It is known that in terms of precipitation there are two maximum peaks in the Antisana region, of which one peak is more marked then the other (Villacis and others, 2008; Vuille and others, 2003b) The higher significant periodicity (80) in the LT isotopic record of the Antisana glacier should correspond to the annual fluctuation induced by precipitation changes, consequently, each reconstructed cycle found represents one year.

Challenges faced in this study was the sampling at uneven depths. A total of 13 samples were analyzed in the first 300 centimeters and 25 samples in the next 250 centimeters (Semiond and others 1998). Furthermore, the first few centimeters of the ice core were not taken due to the poor consistency of the surface snow, which generated uncertainty in subsequent analyses. As for the data gaps, there were 16 data gaps in the density record and 6 data gap in the isotopy record. Therefore, histograms and probability density functions (PDF, Fig. 3) were generated to identify the best sampling resolution for time series required to run the ACF and wavelet analyses. The most frequent value in the histogram and the highest probability in the PDF represents the best resolution to generate a time series. As the dataset is interpolated using the most common observed resolution, dataset changes are minimized.

The logarithmic transformation performed better than the squared transformation as the coefficient of determination was higher (R^2=0.518 > R^2= 0.296). The logarithmic depth transformation was later applied to the isotopic data that had a similar sampling resolution. No further transformations (i.e. polynomial transformations) were performed to further improve the R^2 to avoid overfitting. Simple models should be preferentially used considering the parsimony principle; which states that the simplest solution is usually the best one, therefore complex polynomial functions were avoided. Moreover, the Antisana ice core is superficial and does not experience complex compression forces that apply to ice cores of several hundred meters in length (Dansgaard and Johnsen, 1969; Dansgaard and others, 1993; Di Prinzio and Nasello, 2011; Ginot and others, 2001; Kaspari and others, 2008; Stichler and Schotterer, 2000; Thompson and others, 1982, 1985).

The autocorrelation functions are useful tools for inferring the presence of cycles in a given signal; however, they provide weak a representation when a signal contains multiple periodicities (Hyndman and Athanasopoulos, 2018). Conversely, the ACFs show that the transformations had a visible effect on the correlogram results. The ACF of the original, QT and LT coefficients in the correlograms were dissimilar (Fig. 6a-c). The effectiveness of the transformation cannot be determined with the ACF. The first qualitative approach was to evaluate the slope of the transformed depth-density. A transformation that reduces the slope of the depth-density plot close to zero

indicates that the compression effect of ice accumulation was removed. However, a quantitative evaluation requires a tool such as wavelet analysis.

The wavelet analysis for the LT signal depicts the highest significant period as a straight black line in the heatmap (Fig 7c) suggesting that the LT signal was the best to identify a cycle consistent with annual variability. The rational is that cycles in the isotopic signal should be synchronized with annual precipitation that has a cyclic nature. There are no other events that repeat evenly at this resolution (annual). Then, the highest significant period depicted as a thick black line in the wavelet heatmap should remain parallel to the x-axis (top black line in the heatmap, Fig. 7c). Any departure from a straight line imply that the cycle is becoming larger or smaller like for the QT and untransformed data (top black line in the heatmap, Fig. 7a and 7b). Moreover, the isotopic variability should match the annual processes affecting the amount effect that fluctuates annually (Ginot and others, 2002). That the Antisana experiences little seasonal precipitation change for any given hydrological year (Basantes and others, 2016; Favier and others, 2004; Francou and other, 2004; Ramirez and others, 2003; Semiond and others, 1998; Villacís and others, 2008) does not imply a negligible fluctuation in the isotopic annual signature. For instance, the significant correlation between the precipitation and isotopic data is consistent with the amount effect. Moreover, the 40 and 20 significant periodicities that represent cycles of 6 and 3 months, matched the bimodal nature of precipitation at annual timescales, supporting that the main signal (periodicity=80) is annual.

The wavelet heatmap for the original signal shows indicating that the cycles are reducing their amplitude, which is unexpected for a hydrological year (black line towards smaller periods, Fig. 7a) In contrast, the QT wavelet shows a black line towards higher periodicities (Fig. 7b) indicating that the cycles are gaining amplitude, which again, is unlikely for a hydrological year (Grinsted and others, 2004; Lau and Weng, 1995; Torrence and Compo, 1998). It could be argued that changes in amplitude may fit with processes changing the precipitation patterns due to climate change. However, this scenario is unlikely because the analysis is controlled by the amount effect (seasonally driven) instead of monitoring total rainfall (event driven).

The negative and significant ($r=-0.29$, p-value<0.001 and $R^2=0.0765$) correlation between the precipitation and $\delta^{18}O$ data suggests that the amount effect is the most likely process driving the changes observed in the isotopic signal for the Antisana ice core. As precipitation increases the $\delta^{18}O/\delta^{16}O$ ratio decreases due to enhanced transport of $\delta^{16}O$ isotopes. Enhanced evaporation and advection processes favor light water transport (water containing $\delta^{16}O$ isotopes) over heavy water (containing $\delta^{18}O$ isotopes). Similarly, the correlation between the Antisana and Chimborazo ice cores further validates our results. The correlation between the Antisana and Chimborazo datasets were significant ($r=0.67$, $p<0.001$ and $R^2=0.3973$). Both datasets were evenly sampled to run the correlation using 80 observations per year. Because the correlation was significant between the Antisana and Chimborazo datasets, it can be assumed that similar underlying processes affect both sites. Changes in precipitation modulating the isotopic signal due to the amount effect is the most likely scenario, which is consistent with the literature (Fig. 9b; Hoffmann and others, 2003; Lachniet, 2009; Sturn and others, 2007; Vuille and Werner, 2005). Consequently, the reconstructed trend represented by the dashed lines in Fig. 9b represents an annual periodicity contained in the Antisana isotopic signature that matches the signal from the Chimborazo. Although significant, a correlation coefficient r= 0.67 may not seem high. However, it must be considered that the distance between the Antisana and Chimborazo glaciers is ~130 km. Precipitation events should be localized in each site and local conditions should further induce isotopic variability. Factors such as topography, aspect and the elevation where samples were collected should affect fractionation processes at each site.

All the analyses performed suggest that the main signal for the LT wavelet corresponds to annual cycle driven by the amount effect. Then, the total number of complete cycles identified for

the entire dataset analyzed corresponds to 3.6 cycles (Fig. 10). Our results strongly suggest that age models could be constructed for tropical location based on isotopic data. The analysis indicates that the 13-meter ice core from the Antisana glaciers was deposited over 3.6 years.

6. CONCLUSIONS

The methodology implemented in this article showed that only based on the isotopic record analysis we were able to generate the desired age model that will serve as a reference for future paleoclimatic research on glaciers in the Neotropical region. Furthermore, it shows that annual precipitation is the most likely driver of the annual cycles registered in the isotopic signal from the Antisana ice core. A logarithmic data transformation (LT) was better suited than a squared transformation (QT) to reduce the effects of natural compression of the lower ice layers within the short ice core. The wavelet analysis on logarithmically transformed data provided a consistent periodicity over the analyzed record that corresponds to ~3.6 annual cycles; interannual cycles coinciding with seasonal changes in precipitation were evident and significant. The work developed in this study will need to be reoriented with further studies of ice cores of greater length and location, and with additional statistical analyses to show in more detail the value of uncertainty generated by the model.

Andean glaciers such as Antisana and Chimborazo will support the compression of precipitation variability in the region. The isotopic correlation between the Antisana and Chimborazo records suggests that the amount effect, which is modulated by precipitation enhancement during the austral summer (around November), is likely responsible for the annual cycles observed in the isotope signal. Depleted Isotopes in the Antisana and Chimborazo cores coincide with the southward displacement of the ITCZ and is consistent with isotopic values reported in the literature (Ginot and others, 2010; Martini, 2016).

The results showed that isotopic data can be used to generate age models of tropical ice cores and thus contribute to the understanding of atmospheric dynamics. The development of age models such as the one in this study will allow us to evaluate the temporal influence of climatic and anthropogenic processes in tropical regions in the future.

Acknowledgements

This project was funded by European Union through the consortium AECID - Universidad Regional Amazónica Ikiam (CTC-004-2019, grant to BGV). We also acknowledge funding from the International Joint Laboratory GREAT-ICE, an initiative of the French Institute of Research for Development-IRD (leaders: Thomas Condom, IRD-France and Marcos Villacis, EPN, Quito Ecuador), French Glaciers Observatory Service-GLACIOCLIM (leader: Antoine Rabatel, Univ. Grenoble Alpes, CNRS-INSU, IRD, France) and INAMHI-Glacier Service (leader: Bolivar Caceres, INAMHI, Ecuador)

REFERENCES

Arnaud Y, Muller F, Vuille M and Ribstein P (2001) El Niño-Southern Oscillation (ENSO) influence on a Sajama volcano glacier (Bolivia) from 1963 to 1998 as seen from Landsat data and aerial photography. J Geophys Res-Atmos., **106**(D16), 17773-17784 (doi: 10.1029/2001JD900198)

Baker PA, Fritz SC, Burns SJ, Ekdahl E and Rigsby CA (2009) The nature and origin of decadal to millennial scale climate variability in the southern tropics of South America: the Holocene record of Lago Umayo, Peru. In *Past Climate Variability in South America and Surrounding Regions*, 301-322. Springer, Dordrecht.

Baker PA and Fritz SC (2015) Nature and causes of Quaternary climate variation of tropical South America. *Quat. Sci. Rev.,* **124**, 31-47 (doi: 10.1016/j.quascirev.2015.06.011)

Basantes-Serrano R and 7 others (2016) Slight mass loss revealed by reanalyzing glacier mass-balance observations on Glaciar Antisana 15α (inner tropics) during the 1995–2012 period. J. Glaciol, **62**(231), 124-136 (doi: 10.1017/jog.2016.17)

Bradley RS (1999) *Paleoclimatology: Reconstructing Climates of the Quaternary*, 2nd edn. Academic Press Inc, Massachusetts, 125-186.

Bradley RS, Vuille M, Hardy D and Thompson LG (2003) Low latitude ice cores record Pacific sea surface temperatures. *Geophys. Res. Lett.,* **30**(4) (doi: 10.1029/2002GL016546)

Bradley RS (2015) Paleoclimatology: reconstructing climates of the quaternary, 3rd edn. Academic.

Cabrera M and 7 others (2020) A new method for microplastic sampling and isolation in mountain glaciers: A case study of one Antisana glacier, Ecuadorian Andes. Case Stud. Chem. Environ. Eng., **100051**(*2)* (doi: 10.1016/j.cscee.2020.100051)

Cabodi G, Camurati P and Quer S (2016). A graph-labeling approach for efficient cone-of-influence computation in model-checking problems with multiple properties. *Software: Practice and Experience*, **46**(4), 493-511.

Dansgaard W and Johnsen SJ (1969) A flow model and a time scale for the ice core from Camp Century, Greenland. *J. Glaciol*, **8**(53), 215-223 (doi:10.3189/S0022143000031208)

Dansgaard W and 6 others (1993) Evidence for general instability of past climate from a 250-kyr ice-core record. *Nature*, **364**(6434), 218-220

Delmas RJ (1994). Ice records of the past environment. *Sci. Total Environ.*, **143**(1), 17-30 (doi: 10.1016/0048-9697(94)90530-4)

Di Prinzio CL and Nasello OB (2011) Development of a model for ice core dating based on grain elongation. *Polar Sci.*, **5**(3), 319-326 (doi:10.1016/j.polar.2011.02.001)

Favier V, Wagnon P, Chazarin JP, Maisincho L and Coudrain A (2004) One-year measurements of surface heat budget on the ablation zone of Antizana Glacier 15, Ecuadorian Andes. *J. Geophys. Res. Atmos.*, **109**(D18) (doi: 10.1029/2003JD004359)

Francou B, Ramirez E, Cáceres B and Mendoza J (2000) Glacier evolution in the tropical Andes during the last decades of the 20th century: Chacaltaya, Bolivia, and Antizana, Ecuador. *AMBIO*, **29**(7), 416-422.

Francou B, Vuille M, Favier V and Cáceres B (2004) New evidence for an ENSO impact on low-latitude glaciers: Antizana 15, Andes of Ecuador, 0 28′ S. *J. Geophys. Res-Atmos.*, **109**(D18) (doi: 10.1029/2003JD004359)

Garreaud R, Vuille M and Clement AC (2003) The climate of the Altiplano: observed current conditions and mechanisms of past changes. *Palaeogeogr. Palaeoclimatol. Palaeoecol*., **194**(1-3), 5-22 (doi: 10.1016/S0031-0182(03)00269-4)

Ginot P, Kull C, Schwikowski M, Schotterer U and Gäggeler HW (2001) Effects of postdepositional processes on snow composition of a subtropical glacier (Cerro Tapado, Chilean Andes). *J. Geophys. Res. Atmos.*, **106**(D23), 32375-32386 (doi: 10.1029/2000JD000071)

Ginot P and 7 others (2002) Potential for climate variability reconstruction from Andean glaciochemical records. *Ann. Glaciol.*, **35**, 443-450 (doi: 10.3189/172756402781816618)

Ginot P and 5 others. (2010) Influence of the Tungurahua eruption on the ice core records of Chimborazo, Ecuador. *Cryosphere*, **4**(4), 561-568 (doi: 10.5194/tc-4-561-2010)

Grinsted A, Moore JC and Jevrejeva S (2004) Application of the cross wavelet transform and wavelet coherence to geophysical time series.

Hall ML and 6 others (2017) Antisana volcano: a representative andesitic volcano of the eastern cordillera of Ecuador: petrography, chemistry, tephra and glacial stratigraphy. J. S. Am. Earth Sci., **73**, 50-64.

Henderson KA, Thompson LG and Lin PN (1999) Recording of El Niño in ice core $\delta^{18}O$ records from Nevado Huascarán, Peru. *J. Geophys. Res-Atmos*., **104**(D24), 31053-31065 (doi: 10.1029/1999JD900966)

Hyndman RJ and Athanasopoulos G (2018) *Forecasting: principles and practice*. OTexts.

Hoffmann G and 11 others (2003) Coherent isotope history of Andean ice cores over the last century. *Geophys. Res. Lett*., **30**(4). (doi: 10.1029/2002GL014870)

Kaspari S and 5 others (2008) Snow accumulation rate on Qomolangma (Mount Everest), Himalaya: synchroneity with sites across the Tibetan Plateau on 50–100 year timescales. *J. Glaciol.*, **54**(185), 343-352 (doi: 10.3189/002214308784886126)

Kempf-Leonard K (2004) Encyclopedia of social measurement.

Knüsel S and 8 others (2003) Dating of two nearby ice cores from the Illimani, Bolivia. *J. Geophys. Res-Atmos.*, **108**(D6) (doi: 10.1029/2001JD002028)

Lau KM and Weng H (1995) Climate signal detection using wavelet transform: How to make a time series sing. *B. Am. Meteorol. Soc.*, **76**(12), 2391-2402 (doi: 10.1175/1520-0477(1995)076<2391:CSDUWT>2.0.CO;2)

Lachniet MS (2009) Climatic and environmental controls on speleothem oxygen-isotope values. *Quat. Sci. Rev*., **28**(5-6), 412-432. (doi: 10.1016/j.quascirev.2008.10.021)

Martini M (2016). Sinopsis de los eventos glaciarios del Cuaternario en la Cordillera Oriental de Argentina. Rev. Fac. Cienc. Exactas, Fís. Nat., **3**(2), 125-131.

Mosblech NA and 9 others (2012) North Atlantic forcing of Amazonian precipitation during the last ice age. *Nat. Geosci.,* **5**(11), 817-820.

Moy CM, Seltzer GO, Rodbell DT and Anderson DM (2002) Variability of El Niño/Southern Oscillation activity at millennial timescales during the Holocene epoch. *Nat.*, **420**(6912), 162-165 (doi: 10.1038/nature01194)

Nascimento MN and 8 others (2020) The adoption of agropastoralism and increased ENSO frequency in the Andes. Quat. Sci. Rev., **243**, 106471 (doi: 10.1016/j.quascirev.2020.106471)

Nye JF (1963) Correction factor for accumulation measured by the thickness of the annual layers in an ice sheet. *J. Glaciol.*, **4**(36), 785-788. (doi:)

Paterson WSB (1994) Physics of glaciers. Butterworth-Heinemann.

Ramirez E and 12 others (2003) A new Andean deep ice core from Nevado Illimani (6350 m), Bolivia. *Earth Planet Sc. Lett.*, **212**(3-4), 337-350. (doi: 10.1016/S0012-821X(03)00240-1)

Rodbell DT, Smith JA and Mark BG (2009) Glaciation in the Andes during the Lateglacial and Holocene. *Quat. Sci. Rev*., **28**(21-22), 2165-2212 (doi:)

Santibáñez PA and 6 others (2018) Prokaryotes in the WAIS Divide ice core reflect source and transport changes between Last Glacial Maximum and the early Holocene. *Glob. Chang. Biol*., **24**(5), 2182-2197 (doi: 10.1111/gcb.14042)

Sanz Rodriguez E, Haddad PR and Paull B (2015) *Essential role of ion chromatography in constructing ice core paleoclimatic records*. Chromatography Today, Tasmania 7001, 48-51 p.

Schotterer U and 14 others (2003) Glaciers and climate in the Andes between the Equator and 30° S: what is recorded under extreme environmental conditions?. In Climate Variability and Change in High Elevation Regions: Past, Present & Future, Springer, Dordrecht. 157-175 p.

Semiond H, Francou B, Ayabaca E, de la Cruz A and Chango R (1998) El glaciar 15 del Antizana (Ecuador), Investigaciones Glaciológicas (1994-1997). *Bull. Inst. Fr. Etudes Andin.*, **27**(3)

Stichler W and Schotterer U (2000) From accumulation to discharge: Modification of stable isotopes during glacial and post-glacial processes. *Hydrol. Process*., **14**(8), 1423-1438 (doi: 10.1002/1099-1085(20000615)14:8<1423::AID-HYP991>3.0.CO;2-X)

Stichler W and 7 others (2001) Influence of sublimation on stable isotope records recovered from high-altitude glaciers in the tropical Andes. *J. Geophys. Res. Atmos.*, **106**(D19), 22613-22620 (doi: 10.1029/2001JD900179)

Sturm C, Vimeux F and Krinner G (2007) Intraseasonal variability in South America recorded in stable water isotopes. *J. Geophys. Res-Atmos.*, **112**(D20). (doi: 10.1029/2006JD008298)

Thompson LG, Hastenrath S and Arnao BM (1979) Climatic ice core records from the tropical Quelccaya ice cap. *sci.*, **203**(4386), 1240-1243 (doi: 10.1126/science.203.4386.1240)

Thompson LG 5 others (1982) Geophysical investigations of the tropical Quelccaya ice cap, Peru. *J. Glaciol.*, **28**(98), 57-69 (doi: 10.3189/S0022143000011795)

Thompson LG, Mosley-Thompson E, Bolzan JF and Koci BR (1985) A 1500-year record of tropical precipitation in ice cores from the Quelccaya ice cap, Peru. *Sci.*, **229**(4717), 971-973 (doi: 10.1126/science.229.4717.971)

Thompson LG and 7 others (1995) Late glacial stage and Holocene tropical ice core records from Huascaran, Peru. *sci.*, **269**(5220), 46-50 (doi: 10.1126/science.269.5220.46)

Thompson LG and 11 others (1998) A 25,000-year tropical climate history from Bolivian ice cores. *sci.*, **282**(5395), 1858-1864 (doi: 10.1126/science.282.5395.1858)

Thompson LG (2000a) Ice core evidence for climate change in the Tropics: implications for our future. *Quat. Sci. Rev.*, **19**(1-5), 19-35 (doi: 10.1016/S0277-3791(99)00052-9)

Thompson LG, Mosley-Thompson E and Henderson KA (2000b) Ice-core palaeoclimate records in tropical South America since the Last Glacial Maximum. *J. Quat. Sci.*, **15**(4), 377-394 (doi: 10.1002/1099-1417(200005)15:4<377::AID-JQS542>3.0.CO;2-L)

Thompson LG and 5 others (2003) *Tropical glacier and ice core evidence of climate change on annual to millennial time scales. In Climate variability and change in high elevation regions: Past, present & future*, Springer, Dordrecht. 137-155 p.

Thompson LG, Mosley-Thompson E, Davis ME and Brecher HH (2011) Tropical glaciers, recorders and indicators of climate change, are disappearing globally. *Ann. Glaciol.,* **52**(59), 23-34 (doi: 10.3189/172756411799096231)

Thompson LG and 6 others (2013) Annually resolved ice core records of tropical climate variability over the past~ 1800 years. *sci.*, **340**(6135), 945-950 (doi: 10.1126/science.1234210)

Thorsteinsson T, Kipfstuhl J and Miller H (1997) Textures and fabrics in the GRIP ice core. J. Geophys. Res. Oceans, **102**(C12), 26583-26599

Torrence C and Compo GP (1998) A practical guide to wavelet analysis. *B. Am. Meteorol. Soc.*, **79**(1), 61-78 (doi: 10.1175/1520-0477(1998)079<0061:APGTWA>2.0.CO;2)

Villacís M, Vimeux F and Taupin JD (2008) Analysis of the climate controls on the isotopic composition of precipitation ($\delta^{18}O$) at Nuevo Rocafuerte, 74.5 W, 0.9 S, 250 m, Ecuador. *C. R. Geosci.*, **340**(1), 1-9 (doi: 10.1016/j.crte.2007.11.003)

Vimeux F, Gallaire R, Bony S, Hoffmann G and Chiang JC (2005) What are the climate controls on δD in precipitation in the Zongo Valley (Bolivia)? Implications for the Illimani ice core interpretation. *Earth Planet. Sci. Lett.*, **240**(2), 205-220 (doi: 10.1016/j.epsl.2005.09.031)

Vimeux F and 6 others (2009) Climate variability during the last 1000 years inferred from Andean ice cores: A review of methodology and recent results. Palaeogeogr. Palaeoclimatol. Palaeoecol., **281**(3-4), 229-241 (doi: 10.1016/j.palaeo.2008.03.054)

Vuille M, Bradley RS, and Keimig F (2000) Climate variability in the Andes of Ecuador and its relation to tropical Pacific and Atlantic sea surface temperature anomalies. J. Clim., **13**(14), 2520-2535 (doi:)

Vuille M, Bradley RS, Werner M, Healy R and Keimig F (2003a) Modeling $\delta^{18}O$ in precipitation over the tropical Americas: 1. Interannual variability and climatic controls. *J. Geophys. Res. Atmos.*, **108**(D6) (doi: 10.1029/2001JD002038)

Vuille M, Bradley RS, Werner M, Healy R and Keimig F (2003b) Modeling $\delta^{18}O$ in precipitation over the tropical Americas: 2. Simulation of the stable isotope signal in Andean ice cores. *J. Geophys. Res. Atmos.*, **108**(D6) (doi: 10.1029/2001JD002038)

Vuille M and Werner M (2005) Stable isotopes in precipitation recording South American summer monsoon and ENSO variability: observations and model results. Clim. Dyn., **25**(4), 401-413.

Vuille M and 6 others (2008) Climate change and tropical Andean glaciers: Past, present and future. Earth-Sci. Rev., **89**(3-4), 79-96 (doi: 10.1016/j.earscirev.2008.04.002)

Yu W and 10 others (2016) δ18O records in water vapor and an ice core from the eastern Pamir Plateau: Implications for paleoclimate reconstructions. EPSL., **456**, 146-156 (doi: 10.1016/j.epsl.2016.10.001)

Wolff EW and 29 others (2010) Changes in environment over the last 800,000 years from chemical analysis of the EPICA Dome C ice core. *Quat. Sci. Rev.,* **29**, 285–295 (doi: 10.1016/j.quascirev.2009.06.013)

APPENDICES

APPENDIX A – [Isotopic and density data by Semiond and others, 1998]

Sample	Depth	Oxygen	Density
1	40	-13,4455	
2	60	-11,8890	0,3
3	90	-16,5096	0,42
4	132	-9,5166	
5	150	-11,4426	
6	160	-14,2518	0,42
7	172	-13,7753	0,44
8	192	-18,2683	0,44
9	202	-21,5973	0,44
10	218	-16,9526	
11	258	-18,5663	0,5
12	268	-15,6273	0,5
13	278	-12,1335	0,65
14	300	-15,9838	
15	336	-18,6308	
16	348	-12,9311	0,48
17	365	-16,0887	0,54
18	372	-15,6063	0,54
19	375	-15,0214	0,49
20	388	-13,2805	0,48
21	390	-13,8583	0,38
22	395	-14,9792	0,52
23	409	-15,0000	0,54
24	416	-14,3139	0,52
25	424	-10,9176	0,48
26	432		0,59
27	437	-14,5213	0,74
28	442	-12,1742	
29	455	-13,3010	0,52
30	467	-13,6103	0,52
31	475	-15,0630	0,58
32	484	-17,0587	0,58
33	492	-16,0258	0,58
34	500	-16,9526	0,53
35	507	-18,5237	0,53
36	516	-19,6147	0,55
37	530	-20,4959	0,48
38	545	-25,0169	0,51
39	550	-25,3239	0,51
40	554	-23,4870	0,51
41	566	-17,0376	

Sample	Depth	Oxygen	Density
42	584	-20,3883	0,49
43	591	-18,7160	0,46
44	602	-19,6575	0,46
45	613	-17,4186	0,52
46	620	-13,9823	
47	629	-15,1464	0,53
48	638	-13,3010	0,58
49	652	-15,3759	0,46
50	660	-15,8162	0,49
51	667	-14,4176	0,49
52	682	-13,1983	0,52
53	691	-15,3759	0,55
54	700	-13,2394	
55	708	-14,4176	0,57
56	715	-12,4806	0,61
57	723	-11,6051	0,63
58	732	-11,5033	0,64
59	742	-12,8082	
60	749	-12,9106	0,56
61	755	-11,8078	0,56
62	762	-13,8583	0,59
63	768	-14,0030	0,59
64	776	-13,5279	0,54
65	784	-12,9926	0,55
66	792	-13,7546	0,57
67	801		0,58
68	807		0,51
69	819	-14,5421	0,61
70	829	-15,0000	0,59
71	837	-19,5076	0,57
72	844		0,57
73	854	-19,2076	
74	867	-16,7839	0,63
75	875	-13,8165	0,59
76	886	-16,3623	0,59
77	908		0,56
78	912	-15,7110	
79	917	-13,6103	0,56
80	928	-12,4806	0,56
81	944	-12,1132	0,54
82	954	-14,0650	0,51

Sample	Depth	Oxygen	Density
83	964	-13,0751	0,51
84	970		0,57
85	974	-11,4831	0,54
86	982	-10,9578	0,54
87	996	-10,7969	0,55
88	1008	-10,8170	0,59
89	1024	-10,5755	0,49
90	1038	-10,9377	0,55
91	1050	-11,0384	0,53
92	1060	-11,5241	0,57
93	1068	-12,3785	0,63
94	1080	-12,9106	
95	1087	-13,2188	0,53
96	1096	-13,6309	0,63
97	1106	-14,3554	0,63
98	1118	-14,3346	0,53
99	1126	-13,1367	0,54
100	1137	-14,4591	0,54
101	1146	-14,0443	0,51
102	1155	-13,1162	0,51
103	1165	-13,5897	0,51
104	1177	-10,7361	0,58
105	1190	-11,2810	0,58
106	1205	-12,4601	0,55
107	1219	-12,3785	0,58
108	1226	-11,5443	
109	1234	-10,7768	0,52
110	1245	-11,4831	0,62
111	1253	-13,1778	0,62
112	1265	-12,8901	0,51
113	1275	-14,0650	0,57
114	1285	-14,8127	0,57
115	1294	-15,3759	0,64
116	1306	-16,6785	0,58
117	1318	-18,9080	0,58
118	1328	-19,4220	
119	1334	-19,3145	0,74
120	1346	-18,5663	0,6
121	1357	-18,2896	0,6

APPENDIX B – [DEGREE PROJECT PROGRAM CODE]

```
#####Used libraries
library("WaveletComp")
library("readxl")
library(ggplot2)
library(tidyverse)
library(modelr)

Dens                                                    # density data of ice core
 Dens<-as.data.frame(read_excel("C:/Users/jaque/Desktop/TESIS/TESIS  JC/Tesis.xlsx",  sheet  =
"Density_OK"))                                          #read density as data.frame

#####Histograms and probability density functions to know interpolation interval
plot(hist(Dens[,1], breaks=30), main = "Histogram", xlab = "Depth range", col = "azure3")
plot(density(Dens[-1,1]), main = "Histogram", xlab = "Depth range", col = "black")
abline(v=9, col=4)

#Density depth interpolated Plot
approx(Dens[,2], Dens[,3], xout=seq(from=60, to=1357, by=9))$x ->depth
approx(Dens[,2], Dens[,3], xout=seq(from=60, to=1357, by=9))$y ->densidad
Dens.9cm <-as.data.frame(cbind(depth,densidad))
Dens.9cm
plot(Dens[,2], Dens[,3], type="l", lwd=4, col=3, xlab="depth (cm)")
lines(Dens.9cm, lty=3, lwd=2)
abline(lm(Dens.9cm[,2]~Dens.9cm[,1]),col=2, lwd=3)
summary(lm(Dens.9cm[,2]~Dens.9cm[,1]))

#Plot at tidyverse
ggplot(Dens.9cm, aes(depth, densidad)) + geom_line()  +  ylab(bquote('Density (g/' ~cm^3*')')) +
xlab(bquote('Depth (cm)')) +  geom_smooth(method='lm')

##### Logarithm adjust to density data
Densx_log<-c(log(Dens.9cm[,1]))
Densy_log<-c(Dens.9cm[,2])
log_dens<-as.data.frame(cbind(Densx_log, Densy_log))
plot(log(Dens.9cm[,1]),Dens.9cm[,2] , type="l",  lwd=2, xlab="log(depth)", ylab="Ice density")
abline(lm(Dens.9cm[,2]~(log(Dens.9cm[,1]))),col=2, lwd=3)
summary(lm((Dens.9cm[,2])~log(Dens.9cm[,1]) ))

#Plot at tidyverse
ggplot(log_dens, aes(Densx_log, Densy_log)) + geom_line() +  ylab(bquote('Density (g/' ~cm^3*')'))
+ xlab(bquote('Depth [log(cm)]')) +  geom_smooth(method='lm')

##### Squared adjust to density data
Densx_sqd<-c((Dens.10cm[,1])^2)
Densy_sqd<-c((Dens.10cm[,2]))
cua_dens<-as.data.frame(cbind(Densx_sqd, Densy_sqd))
plot(cua_dens[,1],cua_dens[,2] , type="l",  lwd=2, xlab="cua(depth)", ylab="Ice density")
```

```
abline(lm(Dens.10cm[,2]~(ci)),col=2, lwd=3)
summary(lm((Dens.10cm[,2])~ci ))

# Plot at tidyverse
ggplot(cua_dens, aes(Densx_sqd, Densy_sqd)) + geom_line() +
  ylab(bquote('Density (g/' ~cm^3*')')) + xlab(bquote('Depth ('~cm^2*')')) +
  geom_smooth(method='lm')

################################################################################

# Autocorrelation functions in isotopic data (original and adjusted)
##Original
Auto_0=approx(Oxy.10cm$depth,Oxy.10cm$oxygen, xout =seq(40,1351, length.out = 350))
y0<-data.frame(Auto_0$x,Auto_0$y)
points(y0, col=2)
acf(y0$Auto_0.y, lag.max = 351, main= "Original signal", xlab= "Lag", ylab="ACF")

#Squared
Auto_2=approx(cua_oxy$a,cua_oxy$b, xout =seq(1600,1825741.44, length.out = 350))
y2<-data.frame(Auto_2$x,Auto_2$y)
points(y2, col=2)
acf(y2$Auto_2.y, lag.max = 351, main= "Squared signal", xlab= "Lag", ylab="ACF")

# Logarithm
Auto_1=approx(log_oxy$e,log_oxy$f, xout =seq(3.69,7.20, length.out = 350))
y1<-data.frame(Auto_1$x, Auto_1$y)
points(y1, col=2)
acf(y1$Auto_1.y, lag.max = 351, main= "Natural logarithm signal", xlab= "Lag", ylab="ACF")

################################################################################

##Interval interpolation of logarithm isotopic data
head(Dens)
log(Dens[,2])->depth.log
plot(depth.log, Dens[,3], type="b")
ldd<-c(0)
for (i in 2:105) {
  depth.log[i]-depth.log[i-1]->ldd[i-1]
}
hist(ldd, breaks=60)
plot(density(ldd), col="grey60", lwd=3)
abline(v=0.01034, lty=2)
abline(v=0.012, lty=2, col=2)
approx( depth.log, Dens[,3], xout= seq( from=4.09, to=7.21, by=0.012))$x->depth.log.i
approx( depth.log, Dens[,3], xout= seq( from=4.09, to=7.21, by=0.012))$y->densidad.log.i
dens.log.i <-as.data.frame(cbind(depth.log.i, densidad.log.i))
plot(dens.log.i, type="l" )
```

```
# Logarithm adjust to isotopic data
O18 <- as.data.frame(read_excel("C:/Users/jaque/Desktop/TESIS/TESIS JC/Tesis.xlsx", sheet = "O18_OK"))
approx((log(O18[,2])), O18[,3], xout= seq(from=3.6888, to=7.2152, by=0.012))$x-O18depth.log
approx((log(O18[,2])), O18[,3], xout= seq(from=3.6888, to=7.2152, by=0.012))$y->O18y.i
O18.log.i<-data.frame(O18depth.log, O18y.i)
plot(log(O18[,2]), O18[,3], type="l", xlab="Depth(cm)", ylab= ~delta*''^18~O)
lines(O18.log.i, type="b", lty=2, col=2)

# Plot at tidyverse
ggplot(O18.log.i, aes(O18depth.log, O18y.i)) + geom_line()+geom_point() +geom_ref_line(h=-14.72,colour = "green", size = 1) +
 ylab(bquote(~delta*''^18~O/~delta*''^16~O)) + xlab(bquote('Depth [log(cm)]'))

####  WAVELET LOGARITHM TRANSFORMATION
my.data <- data.frame(x = O18.log.i[-1,2])
my.w <- analyze.wavelet(my.data, "x",
                        loess.span = 0,
                        dt = 1,
                        dj = 1/32,
                        lowerPeriod = 2,
                        upperPeriod = 128,
                        make.pval = TRUE,
                        n.sim = 100)
wt.image(my.w, color.key = "quantile", n.levels = 250, legend.params = list(lab = "wavelet power levels", mar = 4.7))

wt.avg(my.w, show.legend = F)
abline(h=6.33)  # 2^6.33 IS ABOUT 80 steps making each cycle (1 year)
abline(h=5.31)  # 2^5.31 IS ABOUT 40 steps making each cycle (6 months)
abline(h=4.31)  # 2^5.31 IS ABOUT 20 steps making each cycle (3 months)
reconstruct(my.w,sel.period = c(2^6.33))

##original isotopic data
O18_0 <- as.data.frame(read_excel("C:/Users/jaque/Desktop/TESIS/TESIS JC/Tesis.xlsx", sheet = "O18_OK"))
approx((O18[,2]), O18[,3], xout= seq(from=40, to=1357, by=9))$x->O18depth.raw
approx((O18[,2]), O18[,3], xout= seq(from=40, to=1357, by=9))$y->O18y.raw
O18.raw.i<-data.frame(O18depth.raw, O18y.raw)
plot(O18[,2], O18[,3], type="l", xlab="Depth(cm)", ylab= ~delta*''^18~O)
lines(O18.raw.i, type="b", lty=2, col=2)

#### WAVELET ORIGINAL TRANSFORMATION
my.data <- data.frame(x = O18.raw.i[-1,2])
my.w <- analyze.wavelet(my.data, "x",
                        loess.span = 0,
                        dt = 1,
                        dj = 1/32,
                        lowerPeriod = 2,
```

```
                upperPeriod = 128,
                make.pval = TRUE,
                n.sim = 100)
wt.image(my.w, color.key = "quantile", n.levels = 150,legend.params = list(lab = "wavelet power levels", mar = 4.7))
wt.avg(my.w, show.legend = F)
abline(h=5)  # 2^5
abline(h=4.21)  # 2^4.21
reconstruct(my.w,sel.period = c(2^5))

#### Interval interpolation of squared isotopic data
head(Dens)
((Dens[,2])^2)->depth.cuad
plot(depth.cuad, Dens[,3], type="b")
ldd<-c(0)
for (i in 2:105) {
  depth.cuad[i]-depth.cuad[i-1]->ldd[i-1]
}
hist(ldd, breaks=30)
plot(density(ldd), col="grey60", lwd=3)
abline(v=10500, lty=2)
approx( depth.cuad, Dens[,3], xout= seq( from=3600, to=1841100, by=10500))$x->depth.cua
approx( depth.cuad, Dens[,3], xout= seq( from=3600, to=1841100, by=10500))$y->densidad.cua
dens.cua.i<-as.data.frame(cbind(depth.cua, densidad.cua))
plot(dens.cua.i, type="l" )

# Squared adjust to isotopic data
O18_0 <- as.data.frame(read_excel("C:/Users/jaque/Desktop/TESIS/TESIS JC/Tesis.xlsx", sheet = "O18_OK"))
oxy.cua<-c((O18[,2])^2)
approx(oxy.cua, O18[,3], xout= seq(from=1600, to=1841449,  by=10500))$x->O18depth.cua
approx(oxy.cua, O18[,3], xout= seq(from=1600, to=1841449,  by=10500))$y->O18y.cua
O18.cua.i<-data.frame(O18depth.cua, O18y.cua)
plot(oxy.cua, O18[,3], type="l", xlab="Depth(cm)", ylab= ~delta*''^18~O)
lines(O18.cua.i, type="b", lty=2, col=2)

# Plot at tidyverse
ggplot(O18.cua.i, aes(O18depth.cua, O18y.cua)) + geom_line()+geom_point() +geom_ref_line(h=-14.72,colour = "green", size = 1) + ylab(bquote(~delta*''^18~O/~delta*''^16~O)) + xlab(bquote('Depth ('~cm^2*')'))

#### WAVELET SQUARED TRANSFORMATION
my.data <- data.frame(x = O18.cua.i[-1,2])
my.w <- analyze.wavelet(my.data, "x",
                loess.span = 0,
                dt = 1,
                dj = 1/32,
                lowerPeriod = 2
```

```
                upperPeriod = 128,
                make.pval = TRUE,
                n.sim = 100)
wt.image(my.w, color.key = "quantile", n.levels = 250, legend.params = list(lab = "wavelet power levels", mar = 4.7))
wt.avg(my.w, show.legend = F)
abline(h=5.52)  # 2^5
abline(h=4.4)  # 2^4.21 I
reconstruct(my.w,sel.period = c(2^5.52))

############PRECIPITATION vs ISOTOPY
O18 <- as.data.frame(read_excel("C:/Users/jaque/Desktop/TESIS/TESIS JC/Tesis.xlsx", sheet = "O18_OK"))
approx((log(O18[,2])), O18[,3], xout= seq(from=3.6888, to=7.2152,  by=0.012))$x->O18depth.log
approx((log(O18[,2])), O18[,3], xout= seq(from=3.6888, to=7.2152,  by=0.012))$y->O18y.i
O18.log.i<-data.frame(O18depth.log, O18y.i)
plot(log(O18[,2]), O18[,3], type="l", xlab="Depth(cm)", ylab= ~delta*''^18~O) #original
lines(O18.log.i, type="b", lty=2, col=2)  #interpolated

###Sampling points (LT isotopic signal)
A1=approx(O18.log.i$O18depth.log,O18.log.i$O18y.i, xout =seq(3.68,7.21, length.out = 100))
y<-data.frame(A1$x,A1$y)
points(y, col=2)

###Precipitation data
O4 <- read_excel("C:/Users/jaque/Desktop/TESIS/O18.xlsx", sheet = "P_Mica")
plot(O4, type="l")
b1=approx(O4$x,O4$y, xout =seq(1.6,3.89, length.out = 100))
x<-data.frame(b1$x,b1$y)
points(x, col=2)

attach(y)
attach(x)
a<-data.frame(x$b1.y, y$A1.y)
colnames(a)<-c("Isotopic signal","Precipitation")

################################CORRELATION
library(psych)
attach(a)
pairs(a)
pairs.panels(a, main="Correlation",hist.col="green")
cor(a)
summary(lm((a[,2])~(a[,1]) ))

########## ANTISANA vs CHIMBORAZO
read.csv(file="C:/Users/jaque/Desktop/TESIS/Anti_Chimbo/Antisana_Chimborazo.csv",
header=T)->Anti.Ch
```

```
cor.test(Anti.Chim$D18Chim,Anti.Chim$D18Anti, method = "pearson")
cor.test(Anti.Chim$D18Chim, Anti.Chim$WaveYrAnti)
pairs(Anti.Chim)
Anti.Chim
plot(Anti.Chim$D18Chim,Anti.Chim$D18Anti)
summary(lm(Anti.Chim[,5]~Anti.Chim[,4]))

plot(Anti.Chim$yr, Anti.Chim$D18Chim, col=3, lwd=2, type="l")

lines(Anti.Chim$yr, Anti.Chim$D18Anti)
lines(Anti.Chim$yr, Anti.Chim$WaveYrAnti, lty=2)

dim(Anti.Chim)

tama<-4

op <- par(mar = c(5,4.5,4,2) + 0.1)
plot(c(1996,1992), c(-08,-25), type="n", xlab="Years", ylab=expression(delta~O^{-18} ))
par(op)
lines(Anti.Chim$yr, Anti.Chim$D18Anti, lwd=tama, col="tomato")
lines(Anti.Chim$yr, Anti.Chim$D18Chim, lwd=tama, col="cyan3")
lines(Anti.Chim$yr, Anti.Chim$WaveYrAnti, lty=2, lwd=2)
text(1995,-20, labels=c("Antisana"), col="tomato", cex=1.6)
text(1995,-22, labels=c("Chimborazo"), col="Cyan3", cex=1.6)
text(1996,-9, labels=c("B"), cex=1.6)


gg<-ggplot(Anti.Chim, aes(yr)) +
  geom_line(aes(y = D18Anti , colour = "Antisana", size="f")) +  geom_line(aes(y = D18Chim , colour
= "Chimborazo", size="f")) +  scale_colour_manual("Curve",                    values = c("Antisana" =
"lightblue","Chimborazo"= "orange")  )+  scale_size_manual(values=c("f"=1.5))
gg + guides(size = FALSE)
```